The effect of ion-surface and ion-bulk interactions during hydrogenated amorphous silicon deposition

The effect of ion-surface and ion-bulk interactions during hydrogenated amorphous silicon deposition

A. H. M. Smets,[a] W. M. M. Kessels, and M. C. M. van de Sanden
Department of Applied Physics, Eindhoven University of Technology, P.O. Box 513, 5600 MB Eindhoven, The Netherlands

(Received 8 March 2006; accepted 15 August 2007; published online 11 October 2007)

The ion-bombardment induced surface and bulk processes during hydrogenated amorphous silicon (*a*-Si:H) deposition have been studied by employing an external rf substrate bias (ERFSB) in a remote $Ar-H_2-SiH_4$ expanding thermal plasma (ETP). The comparison of the ETP chemical vapor deposition without and with ERFSB enables us to identify some important ion-surface and ion-bulk interactions responsible for film property modifications. Employing ERFSB creates an additional growth flux and the low energetic ions deliver an extra 5–10 eV per Si atom deposited at typical deposition rates of 10–42 Å/s which is a sufficient ion dose to modify the film growth. It is demonstrated that the extra surface and bulk process during *a*-Si:H growth, induced by the additional ion bombardment, provide an extra degree of freedom to manipulate the *a*-Si:H microstructure. An ion-film interaction diagram is introduced, which is used to discriminate ion-surface interactions from ion-bulk interactions. According to this ion-film interaction diagram, the *a*-Si:H grown with ERFSB can be roughly classified in three phases. In phase I the only ion-surface process activated is Si surface atom displacement. In phase II also ion-induced Si bulk atom displacement is sufficiently activated, whereas in phase III ion-induced Si atom sputtering is significant. Phase I is characterized by a reduction in the nanosized void density, a reduction in defect density, and an improvement of the photoresponse. We find that the Si surface displacement is the process responsible for various improvements of the material properties via the enhanced surface migration. Phase II is characterized by an enhancement of vacancy incorporation. In accordance with the introduced ion-film interaction diagram, the Si atom bulk displacement process is responsible for the incorporation of additional vacancies. Phase III is characterized by the decrease in growth flux and the increase in void density. The significant contribution of ion-sputtering processes is responsible for the effects observed in phase III. © *2007 American Institute of Physics*. [DOI: 10.1063/1.2786873]

I. INTRODUCTION

The insights in the precursor flux and its interactions with the surface are crucial in the understanding of thin hydrogenated silicon (Si:H) film deposition from a SiH_4 or SiH_4/H_2 plasma. The composition of the growth flux, and the interaction of the specific radicals, ions, and clusters with the growth surface and the surface processes are crucial in the determination of the material properties and the exact nature of the Si:H films. The two most important and best defined Si:H material phases are the amorphous (*a*-Si:H) and nano-/microcrystalline[1] (μc-Si:H) phase, whereas at growth conditions at the transition from *a*-Si:H to μc-Si:H, some slightly different material phases such as protocrystalline[2] (pc-Si:H) and polymorphous[3] (pm-Si:H) have been classified. In general a SiH_3 dominant radical flux without polysilane radicals leads to growth of highly stabilized *a*-Si:H.[4] A significant amount of atomic hydrogen in the growth flux results in μc-Si:H growth,[2] whereas it is suggested that if nanosized crystalline clusters created in the plasma are incorporated in the Si:H film under conditions near the *a*-Si:H$\rightarrow\mu$c-Si:H transition, a different Si:H phase, the so-called pm-Si:H, can be obtained.[3] In contrast to the insight in the role of radicals to the Si:H growth and the resulting Si:H nature, the insight in the effect of ion bombardment during Si:H growth is rather poor as beneficial and damaging effects have been reported.[5–16]

Ions can have a considerable amount of kinetic energy in comparison to neutrals, because they can be accelerated using an electric field. Therefore in contrast to neutrals, ions can enhance or induce processes such as surface species migration, displacement of surface and bulk atoms, and sputtering.[17,18] The typical binding energy between atoms in a film equals several eV, and as a consequence an ion energy dose of >5 eV per deposited atom is required to significantly modify the film properties.[17] To what extent the energy of an ion is transferred to the surface and bulk atoms depends on the ion-surface or ion-bulk interaction mechanism. The yield of these interactions depends on the ion/atom arrival rate, the ion energy and the ratio between the mass of the ion and the surface or bulk atoms. Consequently, the broad distribution of ion energies in a deposition plasma makes the experimental identification of ion-surface and ion-bulk interactions even more difficult under the consideration that one single

[a]Present address: Research Center for Photovoltaics, National Institute of Advanced Industrial Science and Technology, Central 2, 1-1-1 Umezono, Tsukuba, Ibaraki, Japan. Electronic mail: arno.smets@aist.go.jp

type of ion can have many different interactions with the depositing film depending on its impact energy.

For the μc-Si:H growth conditions it has been recognized that the energies of the surface bombarding ions have to be below a certain threshold energy to prevent amorphization of the Si:H film.[5,6] The role of ion bombardment during hydrogenated amorphous silicon (*a*-Si:H) growth and its effect on the material properties seem to be more complex. Here we will give a brief overview of the important results reported in literature on the influence of ion bombardment on the *a*-Si:H growth. In general the deposition conditions with ion bombardment result in denser *a*-Si:H films as demonstrated for dc discharges, rf-plasma enhanced chemical vapor deposition (rf-PECVD), very high frequency PECVD (VHF-PECVD), and electron cyclotron resonance CVD (ECR-CVD) with substrate bias.[7–10] Hamers *et al.*[9] showed that good structural properties (a minimum incorporation of nanosized voids) can be obtained when the ions deliver an energy higher than 5 eV per deposited Si atom in a VHF-PECVD silane plasma. This result implies that significant film growth modification by ions depends on the typical binding energies of the Si–Si and Si–H bonds in the *a*-Si:H, which are both around 3 eV.[11] For *a*-Si:H deposition by means of a dc discharge and ion-beam-assisted evaporation an increase in the low stretching mode (LSM) absorption around 1980–2010 cm^{-1},[7,8,12] with increasing ion-bombardment energy, has been observed. Furthermore, two different research groups report on the fact that a minimum bulk defect density of *a*-Si:H is obtained in a specific ion energy range of 25 up to 40 eV for *a*-Si:H deposited using rf-PECVD at $R_d < 2$ Å/s.[13,14] For ECR deposition it has been demonstrated that the optoelectronic properties such as the photoresponse improve by employing a substrate bias,[10] whereas *a*-Si:H deposited using silicon evaporation assisted by a low-energy ion source results in optimum photoresponse at ion energies of 100–200 eV.[15] For VHF depositions with controlled electron and ion energy distributions a two order of magnitude higher hole drift mobility around an ion energy of 20–25 eV has been reported.[16]

It is difficult to compare the results mentioned above, as these results are obtained for different techniques and different deposition conditions. Furthermore, the results are discussed in terms of general growth process indicators such as removing excess H, removing weaker bonds, removing structural defects, and etching. Despite the fact that many ion-surface interactions on the Si network and its surface have been thoroughly studied, such as the ion-induced displacement of surface Si atoms and bulk Si atoms[18,19] or Si sputtering,[20] these well known ion-surface interactions are barely mentioned in the literature on Si:H growth studies.

The most widespread method used to deposit *a*-Si:H from a growth flux of neutral radicals and ions is parallel plated rf-PECVD and VHF-PECVD. The ion energy distribution (IED) in these plasmas has depending on the pressure a so-called bimodal distribution, with maximum ion population near the minimum and maximum ion energies.[21] The energy flux to the substrate is completely different for the deposition of *a*-Si:H by means of a remote plasma, as here the neutral radicals dominate the growth flux. The energy of ions bombarding a grounded substrate in a remote plasma is extremely low since the ions are only accelerated by the induced substrate self-biasing. The low energetic ion bombardment of remote plasmas is a crucial advantage for the study of the effect of ion bombardment on the film growth: by employing an external bias on the substrate in a remote plasma, the ion energy can be manipulated without significantly manipulating the flux of neutral radicals towards the substrate. Examples of remote plasmas are ECR-CVD and the expanding thermal plasma chemical vapor deposition (ETP-CVD). In these plasmas the typical energies of the surface bombarding ions are <10 eV (Ref. 22) for ECR and <2 eV for ETP-CVD.[23]

Another important feature of a remote plasma is the large freedom in plasma parameters. Hence, a remote deposition technique, such as ETP, has easy access to ultrahigh deposition rates of ~ 100 Å/s,[24,25] compared to typical deposition rate of 1–2 Å/s for conventional rf-PECVD. However, since the radical-surface interactions dominate the *a*-Si:H growth during remote plasma deposition, the preservation of the material properties of *a*-Si:H deposited by means of remote plasmas at high deposition rate requires higher substrate temperatures.[22,24–27] From an industrial viewpoint it is desirable to deposit at substrate temperatures as low as possible ($T_{sub} < 250$ °C) and at deposition rates as high as possible. The creation of an additional ion bombardment in remote plasmas is an alternative route to transfer additional energy to the growing film. By employing an external rf substrate bias (ERFSB) during *a*-Si:H growth from a remote plasma, the combination of high deposition rates and "low" energetic ion energies of some tens of eV can be exploited. For example, in the case of epitaxy Si growth from Si^+ ions an ion-energy-temperature synergism has been proposed.[28] If the important ion-surface and ion-bulk interactions during *a*-Si:H growth would be known, the fundamental question arises whether all ion-surface and ion-bulk interactions are exchangeable with the substrate temperature, or in other words whether ion bombardment is a good replacement for substrate temperature.

The choice of using the ETP with ERFSB to study the ion effect provides two practical advantages: First, by comparing the ETP deposition with and without ERFSB (ion bombardment <2 eV) the effect on the growth of the additional ion bombardment can be better observed, which makes the determination whether any of the above mentioned well known ion-surface interactions are contributing to *a*-Si:H growth much easier. The second advantage of using the ETP with ERFSB configuration is the fact that the (a) composition of the plasma beam and (b) the *a*-Si:H growth under pure ETP conditions are well characterized: (a) The dominant growth radicals under pure ETP conditions have been identified. It has been demonstrated that the SiH_3 radical contributes dominantly ($>90\%$) to the *a*-Si:H growth, whereas other species such as SiH_2, SiH (2%–3%), Si ($<0.5\%$), and ionic clusters ($<5\%$) have a minor contribution to the growth.[29,30] Any contribution of polysilane molecules, negative ions, and dust particles have not been observed within the detection limits of the diagnostics used.[29,30] The energy of the substrate bombarding ions, i.e., the substrate self-

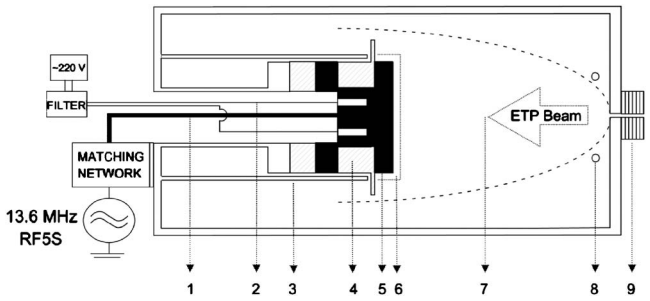

FIG. 1. Schematic presentation of the ETP plasma chamber in the ERFSB configuration: (1) the copper strip going from the output of the match box to the substrate holder, (2) the power supply of the substrate heating elements with Belling Lee SF4200-16/01 filter, (3) rf shield around substrate yoke, (4) isolating glass tubes, (5) substrate holder, (6) rf plasma sheath, (7) expanding thermal plasma beam, (8) silane injection ring, and (9) cascaded arc plasma source.

biasing, is typically well below 2 eV. (b) Under these well-defined growth conditions higher substrate temperatures are needed to preserve good material properties at the higher deposition rates obtained. The material quality is mainly determined by the nanosized void incorporation during growth, which is subsequently a result of the competition between surface diffusion and arrival rate of the precursor species.[25]

In this paper we present a study of the additional ion bombardment generated by employing an ERFSB in an ETP under well-defined *a*-Si:H deposition conditions. Furthermore, we will introduce a general ion-film interaction diagram, which is based upon the fundamental ion-surface and ion-bulk interactions. Using this ion-phase diagram some beneficial and damaging ion-surface and ion-bulk interactions on the *a*-Si:H growth by means of ETP with ERFSB have been identified. Furthermore, to which extent the substrate temperature and ion energies of some specific ion-surface and ion-bulk interaction are exchangeable will be discussed in more detail, as well. The details on the ERFSB setup are presented in Sec. II. The effects of the additional ion bombardment on the growth flux, microstructural properties, and material defects are presented in Sec. III. In sec. IV we introduce a general ion-film interaction diagram including well-known ion-induced surface and bulk processes. The ion-surface interactions responsible for the material modifications are identified by means of this diagram.

II. EXPERIMENT

The ETP technique is based on the generation of an Ar-H_2 plasma in a thermal plasma source, the so-called cascaded arc, which operates at typical pressures of 0.2–0.6 bar.[23] In these deposition conditions the arc operates as an intense atomic hydrogen source. The created Ar-H_2 plasma expands into a low pressure chamber. In the expansion the electron temperature is reduced to 0.1–0.3 eV. The precursor gas SiH_4 is admixed in the low pressure chamber just behind the source exit via an injection ring (see Fig. 1). The silane is dissociated by the atomic hydrogen into mainly SiH_3 radicals. Details on the remote ETP technique can be found in Refs. 23 and 24.

The additional ion bombardment is generated by applying 13.56 MHz rf power to the substrate holder.[31] The

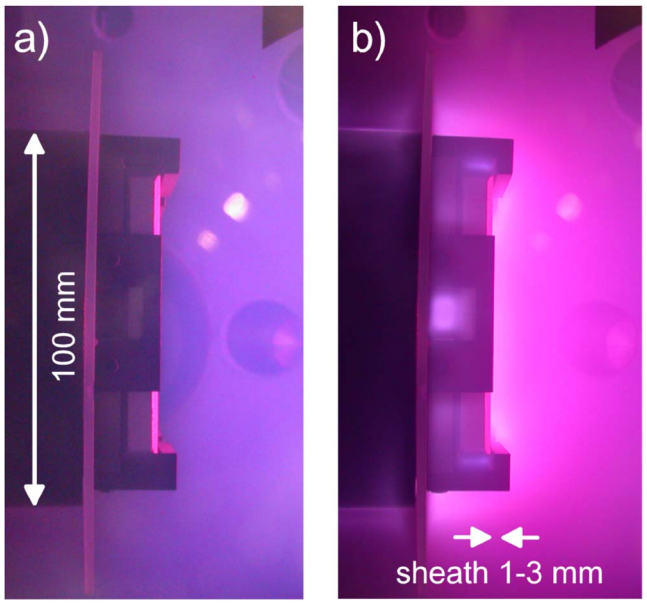

FIG. 2. (Color online) The substrate holder in the ETP operated on Ar–H_2–SiH_4 (a) without and (b) with ERFSB.

ERFSB setup is depicted in more detail in Fig. 1. The rf power has been generated with a RFPP power supply (type RF5S) and an *L*-type matching network has been used for impedance matching. The output of the matching network is coupled to a copper strip. The end of the copper strip is attached to the back side of the substrate holder. The ground of the matchbox is directly connected to the grounded vessel wall. Since the heating elements are directly mounted at the back side of the biased substrate holder, a Belling Lee SF4200-16/01 filter has been used to prevent any rf leakage current via the element's power supply lines. The holes in the substrate yoke are filled with glass (shaded areas in Fig. 1) to prevent the confinement of dense plasma spots in so-called hollow cathodes. The black colored part of the substrate holder, as depicted in Fig. 1, is the total rf biased electrode, whereas the total wall of the vessel can be considered as the grounded electrode.

In Fig. 2, two pictures of the side view of the substrate holder during ETP exposure is shown without [Fig. 2(a)] and with ERFSB [Fig. 2(b)]. The rf power (P_{rf}) is varied from 0 to 140 W which results in typical bias voltage V_{dc} in the range of −10 V down to −200 V.[31] The typical thickness of the dark rf plasma sheath at the substrate holder ranges from 1 to 3 mm for an Ar-H_2-SiH_4 plasma depending on P_{rf} and pressure. In the region between the dark sheath (~1–2 mm) and the bulk plasma, the plasma emits additional light, which indicates additional plasma creation or electron heating due to the ERFSB bias.

The *a*-Si:H films have been deposited on *c*-Si for the microstructural studies and on Corning 7059 glass for the defect density and conductivity measurements. Since glass is an insulator, this could result in a slightly different V_{dc} on the glass substrate as on c-Si under the same rf power employed. Under the conditions used in this paper ($-200\ V < V_{dc} < 0\ V$) the ion flux does not exceed a few times $10^{15}\ cm^{-2}\ s^{-1}$. This results in a V_{dc} on glass which is at maxi-

mum 2 V lower than on c-Si, a difference that can be considered as insignificant. The results presented in this paper have been deposited under two conditions: A and B. These conditions have typical high deposition rates at which higher substrate temperatures (>250 °C) are required to preserve the material properties when no ERFSB is employed. This makes conditions A and B suitable to study the possible interchangeability of substrate temperature and ion energy. Condition A corresponds to 45 sccs argon, 4 sccs H_2, 3.5 sccs SiH_4, arc current of 21 A at a pressure of 0.14 mbar, and a substrate temperature of 200 °C. The deposition rate varied from 11 Å/s at P_{rf}=0 W (V_{dc}~0 V) up to 17 Å/s at P_{rf}=40 W (V_{dc}~−120 V). Condition B corresponds to 55 sccs argon, 5 sccs H_2, 4 sccs SiH_4, arc current of 32 A at a pressure of 0.18 mbar, and a substrate temperature of 200 °C. The deposition rate varied from 25 Å/s at P_{rf} =0 W (V_{dc}~0 V) up to 42 Å/s at P_{rf}=140 W (V_{dc}~−200 V).

The microstructure of the films has been analyzed by infrared transmission spectroscopy. The infrared transmission measurements provide the refractive index, deposition rate R_d (from the thickness and deposition time), film density, Si growth flux, and the total hydrogen content (c_H) of the films.[33] The microstructural information on the hydrogen incorporated in vacancies and at the surface of nanosized voids has been determined from the LSM (around 2000 cm^{-1}, i.e., hydrogen in vacancies) and the high stretching mode (HSM) (around 2080 cm^{-1}, hydrogen at void surfaces), c_{LSM} and c_{HSM}, respectively.[33]

Transmission-reflection (TR) measurements and dual beam photoconductivity (DBP) are performed on the *a*-Si:H films deposited on Corning glass to measure the subgap absorption. The relative DBP spectra are fitted to the 1.6–1.8 eV range of the TR spectra measured. Finally, the AM1.5 and dark conductivity at room temperature have been measured.

III. RESULTS

A. The effect of ERFSB on the growth flux

The total SiH_4 depletion in the ETP as determined from residual gas analysis by means of mass spectroscopy is typically 10% for the conditions used. The ERFSB depletes locally additional SiH_4 at the biased substrate, which results in about 1% extra depletion to the total SiH_4 depletion in the plasma chamber. We briefly mention here that the change in the plasma beam composition (additional radical production) has been studied for ETP conditions by means of time-resolved cavity ring down spectroscopy (τ-CRDS) by Hoefnagels *et al.*[34] In these experiments the additional creation and loss of Si and SiH_3 radicals in front of the substrate (at ~5 mm) for pulsed ERFSB have been measured. The measurement revealed that Si density increases with a factor 5–6 and that Si atoms are lost via gas phase reactions, whereas the SiH_3 density increases with 60%–80% by employing an ERFSB and is lost dominantly at the surface. Furthermore, a signature of the creation and confinement of clusters at the edge of the plasma sheath on time scales larger than some tens of milliseconds has been observed as well.

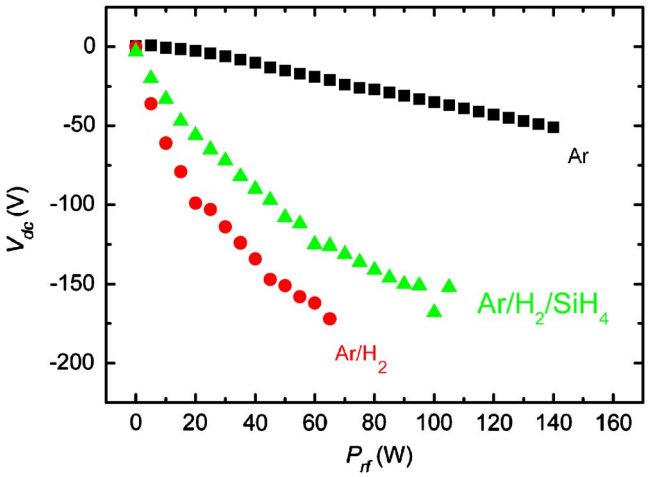

FIG. 3. (Color online) The value of V_{dc} measured at the substrate vs P_{rf} for an Ar, Ar–H_2, and Ar–H_2–SiH_4 plasma.

The measured dc bias voltage V_{dc} on the substrate is shown in Fig. 3 for a pure Ar plasma, an Ar-H_2 plasma, and Ar–H_2–SiH_4 plasma. The grounded electrode, the vessel wall, has during the entire rf cycle a potential of 0 V. As the mobility of the light electrons is always larger than the "heavy ions," the plasma potential is always larger than the electrode potential, i.e., $0 < V_p < V_{max,electrode}$. Due to the asymmetry (the powered electrode is usually smaller than the grounded) and capacitive coupling the average voltage of the powered substrate holder, V_{dc}, is smaller than the grounded vessel wall. The fact that V_{dc} is much lower for the Ar plasma compared to the Ar–H_2 and Ar–H_2-SiH_4 plasma indicates that the ion current and therefore the electron density in the Ar plasma are much higher.[32] For a pure Ar plasma, a linear dependence of the V_{dc} on the rf power P_{rf} is observed, which indicates that all rf power is used for electron heating in the plasma near the substrate and to accelerate the ions in the plasma sheath. Or equivalently, from the relation $P_{rf}=I_{ion}V_{dc}$ it is clear that the ion current I_{ion} is not influenced by the rf power, as the electron density for the remote plasma is already significantly high. (Note that we neglected the power consumed by electron heating, since the energy that an ion gains in the plasma sheath is much larger.) The relation between V_{dc} and P_{rf} for an Ar–H_2 plasma and the Ar–H_2–SiH_4 plasma shows an evident deviation from a linear relationship. This clearly indicates that not all energy is used to accelerate ions within the plasma sheath. Therefore we conclude that electrons heat up in the plasma near the substrate and that a considerable fraction of the rf power is used to create additional plasma (i.e., to create a higher electron density) in front of the substrate surface resulting in additional fragmentation of the H_2 and SiH_4.

For the conditions presented in this paper one ion is available per 6–20 deposited Si atoms. When the plasma sheath is collisionless, every ion brings on average an energy of $\bar{E}_{ion}=e|V_p-V_{dc}|$ to the substrate with V_p the plasma potential. The wall of the deposition setup, the grounded electrode, is much larger (at least hundred times) than the biased substrate electrode. Due to this extreme asymmetric electrode configuration, V_p is mainly pinned by the sheath voltage drop

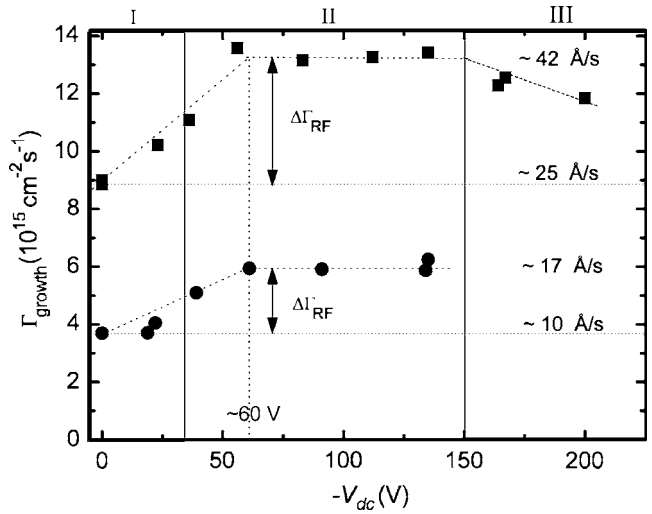

FIG. 4. The Si growth flux Γ_{Si} vs $|V_{dc}|$ for condition A (R_d=10 Å/s) and condition B (R_d=25 Å/s). Phases I, II, and III, as described in the text, are indicated as well.

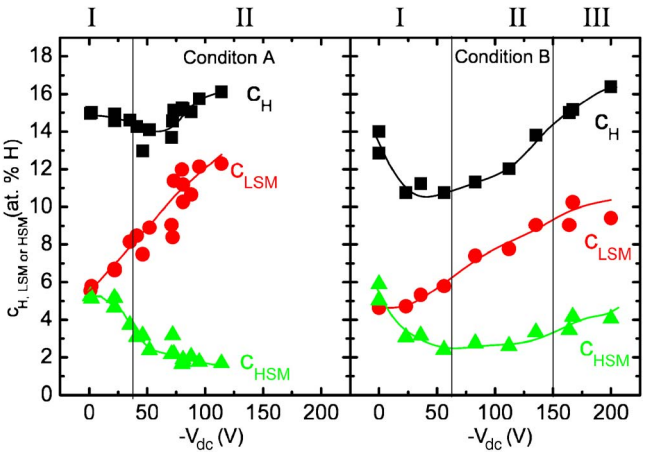

FIG. 5. (Color online) The total hydrogen content c_H (squares), the hydrogen content contributing to the LSM c_{LSM} (circles), and the hydrogen content contributing to the HSM c_{HSM} (triangles) vs the dc voltage V_{dc} for R_d =11 Å/s (condition A) and R_d=25 Å/s (condition B). Phases I, II, and III, as described in the text, are indicated as well.

at this large grounded chamber wall and is typically around +1 up to +2 eV. Therefore we can use in this paper the approximation that $\bar{E}_{ion}=e|V_{dc}|$ in line with Ref. 21. The IED at the substrate position has not yet been measured for the conditions described in this paper. Nevertheless, in the typical pressure range of 14–18 Pa used, the IED of a rf biased electrode has a so-called bimodal shape, i.e., a maximum E_1 below $\bar{E}_{ion}$ and maximum E_2 above $\bar{E}_{ion}$,[21] which does not have to be symmetrical around $\bar{E}_{ion}$. In the remainder of this paper, we will present the data in terms of $|V_{dc}|$. However, we would like to stress that this $|V_{dc}|$ only reflects the averaged energy of the broad distribution of ions around $\bar{E}_{ion}$ and not the width of the energy distribution.

The question remains which ions bombard the surface. Under ETP conditions without ERFSB hydrogen poor ion clusters $Si_nH_m^+$ can contribute up to 5% of the *a*-Si:H growth.[35] With ERFSB these ions are accelerated to the growth surface. Since the ions contain on average around six Si atoms the partial ion/atom arrival ratio of these ionic clusters is roughly ~0.008. The total ion/atom arrival ratio for conditions A and B ranges from 0.05 up to 0.15, meaning that other ions are mainly responsible for the energy transfer to the growth surface. The additional ions created in front of the substrate are most probably SiH_n^+ with n=0–3, H_2^+, H^+, and Ar^+.

In line with the creation of additional radicals and ions, the ERFSB employed creates an additional growth flux next to the creation of additional ion bombardment.[32] Figure 4 shows that the Si growth flux increases versus the V_{dc} for conditions A and B. For reasons, which will be clarified later in the paper, we have defined three phases as indicated in Fig. 4. The Si growth flux increases with $|V_{dc}|$ up to $|V_{dc}|$ <60 V (phase I) while for higher $|V_{dc}|$ values (phase II) the Si growth flux saturates. The generation of an additional growth flux is also observed for *a*-Si:H deposition by remote ECR with ERFSB (Ref. 10) and microwave plasma CVD (MPCVD).[36] For the highest ion bombarding energies $|V_{dc}|$ >150 V, corresponding to phase III, the Si growth flux is slightly decreasing for condition B same as observed for ECR with ERFSB.[10] At V_{dc}=−200 V the Si growth flux is 10% smaller than the growth flux in phase II.

The increase in deposition rate for conditions A and B is 70% and roughly correlates with the additional SiH_3 growth flux created (60%–80%) as measured by CRDS under pulsed ERFSB conditions. Since SiH_3 is the dominant contributor to the *a*-Si:H growth in ETP conditions without ERFSB, the SiH_3 radical remains the dominant contributor to the *a*-Si:H deposition for ETP with ERFSB. In other words the composition of the radical flux to the substrate is not significantly changed utilizing an additional ERFSB.

B. The relation between the microstructure and the additional ion bombardment

The dependences of the total hydrogen content c_H, the hydrogen content contributing to the LSM and HSM, c_{LSM} and c_{HSM}, respectively, are shown in Fig. 5 for deposition conditions A and B. Note that for condition A, V_{dc} has been varied down to −120 V (phases I and II), whereas for condition B the V_{dc} has been varied down to −200 V (phases I, II, and III). The c_{LSM} increases with increasing $|V_{dc}|$ in phase II for both conditions A and B. These results imply that the vacancy incorporation increases with increasing ion-bombardment energy. The same trend has been observed for *a*-Si:H deposition using different deposition techniques,[7,12] demonstrating the generality of the ion-surface interactions which affect the vacancy incorporation.

The c_{HSM} drops already drastically for moderate V_{dc} values of $|V_{dc}|$ (<50 V) in conditions A and B (phase I). For 50 V<$|V_{dc}|$<140 V (phase II) the c_{HSM} slightly decreases with $|V_{dc}|$. These results imply that only a moderate ion bombardment is required to drastically decrease the incorporation of nanosized voids. The films become denser under additional ion bombardment in agreement with the observed densification of *a*-Si:H under increasing ion-bombardment energy using different techniques.[7–10] For higher ion energies,

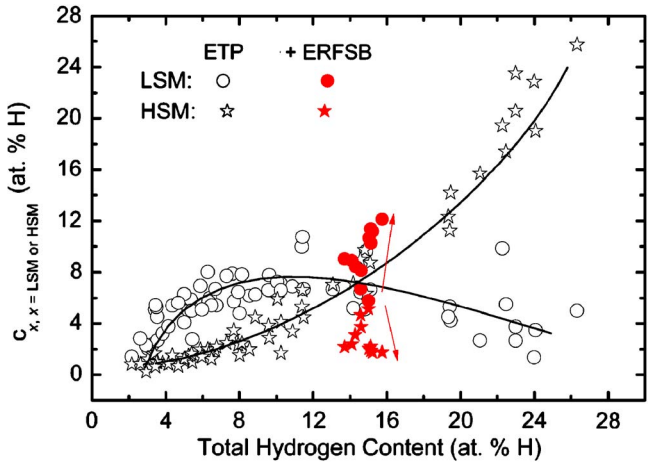

FIG. 6. (Color online) The hydrogen content contributing to LSM c_{LSM} (circles) and HSM c_{HSM} (stars), deposited without (open marks) and with ERFSB (solid marks) in condition A vs the hydrogen content. The data points from the pure ETP conditions are from Ref. 33 and obtained by growth flux and substrate temperature variation. The ERFSB conditions correspond to the rf-power series shown in Fig. 6.

$|V_{\mathrm{dc}}|>150$ V (phase III), the nanosized void density seems to increase slightly with increasing $|V_{\mathrm{dc}}|$ for condition B.

The total hydrogen content as determined using the wagging mode at 640 cm^{-1} is roughly the sum of the hydrogen bonded to the Si at the vacancies and the hydrogen bonded to the Si at the nanosized void surfaces.[25] The total hydrogen content shows for both conditions A and B a minimum around $|V_{\mathrm{dc}}|\sim 50$ V up to ~ 70 V (at the transition from phase I to II), since the vacancy incorporation is increasing and the void incorporation is decreasing with increasing $|V_{\mathrm{dc}}|$.

In Fig. 6 the c_{LSM} (reflecting the hydrogen bonded at vacancies) and the c_{HSM} (reflecting the nanosized voids) are shown as a function of the total hydrogen content. Figure 6 demonstrates that the deposition under pure ETP conditions (taken from Ref. 33), i.e., conditions in which the surface-neutral radical interactions are dominant, results in material having a fixed void and vacancy density at certain hydrogen content. Figure 6 demonstrates that if an ERFSB is employed the microstructure breaks out of the fixed microstructure for ETP growth without ERFSB. In other words the ERFSB provides us an extra degree of freedom in the variety of *a*-Si:H microstructures which can be obtained.

C. Effect of ion bombardment on the bulk defects

In Fig. 7 the results of TR and DBP measurements of samples deposited in condition A are shown. The subgap absorption corresponds to the optoelectronic active defects in the *a*-Si:H network. The subgap absorption is rather high for the ETP without ERFSB condition. Employing a moderate rf bias with $V_{\mathrm{dc}}=-46$ V, corresponding to phase I, results in a drastic reduction of the subgap absorption of the *a*-Si:H material. For phase II, $|V_{\mathrm{dc}}|>50$ V the subgap absorption remains constant at a slightly higher value than the minimum in phase I. This trend is also reflected in Fig. 8 in which the Urbach energy and the absorption coefficient at 1.2 eV are plotted versus V_{dc}. These results are in agreement with the

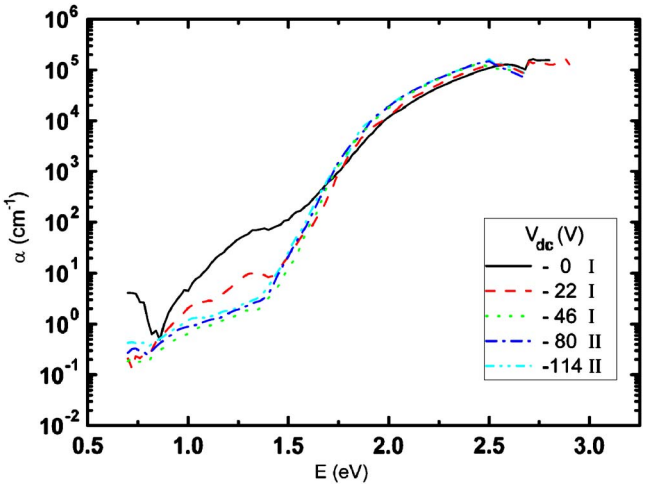

FIG. 7. (Color online) The absorption coefficient of the *a*-Si:H measured by means of TR and DBP for films deposited under condition A at various P_{rf}.

minimum defect densities in *a*-Si:H found around $\bar{E}=25-40$ eV deposited by rf-PECVD and VHF-PECVD at lower deposition rates ($R_d<2$ Å/s).[13,14]

The AM1.5 conductivity $\sigma_{\mathrm{AM1.5}}$, the dark conductivity at room temperature σ_{dark}, and the photoresponse versus V_{dc} are shown in Fig. 9 for *a*-Si:H films deposited under condition A. Only a moderate V_{dc} (phase I) is required to slightly improve the AM1.5 conductivity, to drastically lower the dark conductivity, and to consequently increase the photoresponse. A photoresponse over 10^6 is obtained under ERFSB conditions for $|V_{\mathrm{dc}}|\sim 20$ up to 40 eV. An improvement of the *a*-Si:H photoresponse under ion bombardment has also been observed by others.[10,15]

D. Interchangeability of substrate temperature and ion bombardment

To study to which extent ion bombardment and substrate temperature are interchangeable, films have been deposited as a function of the substrate temperature at conditions A and B without and with ERFSB ($V_{\mathrm{dc}}=-60$ V, i.e., $P_{\mathrm{rf}}=40$ W at

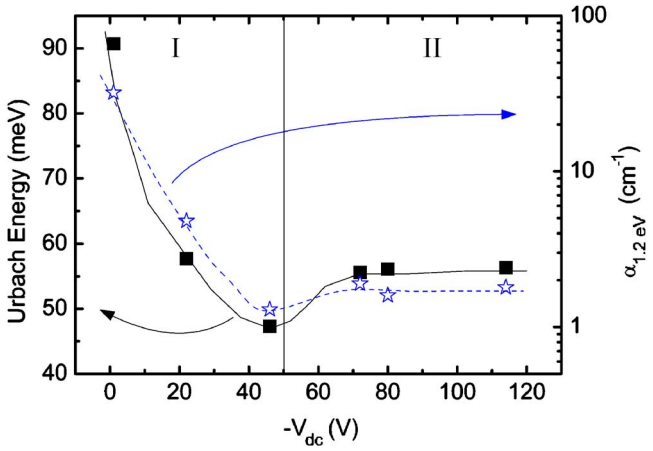

FIG. 8. (Color online) The Urbach energy (solid marks) and the absorption coefficient at 1.2 eV (open stars), both obtained by means of TR and DBP measurements vs $-V_{\mathrm{dc}}$. Phases I and II, as described in the text, are indicated as well.

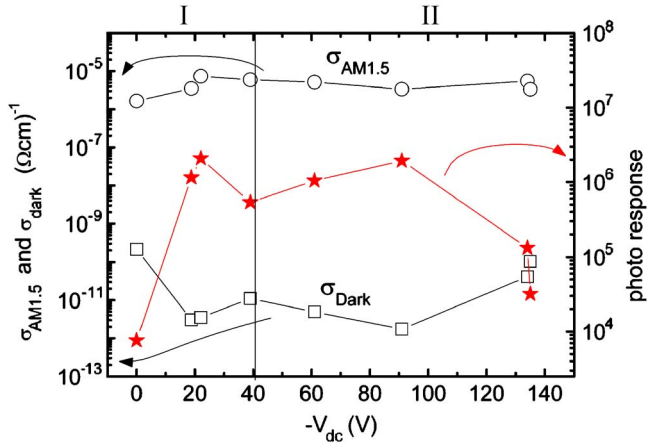

FIG. 9. (Color online) The AM1.5 conductivity (open circles), the dark conductivity (open squares), and photoresponse (solid stars) vs the dc voltage (V_{dc}) for condition A. Phases I and II, as described in the text, are indicated as well.

condition A and P_{rf}=60 W at condition B). The c_H, c_{LSM}, and c_{HSM} are plotted versus the substrate temperature in Fig. 10 for conditions A and B. The solid marks correspond to ETP depositions without ERFSB and the open marks correspond to ETP depositions with ERFSB. In Fig. 11 the differences between deposition with and without ERFSB are shown for condition A (open circles) and condition B (solid stars), where $\Delta c_H = c_{H,+ERFSB} - c_{H,ETP}$, $\Delta c_{LSM} = c_{LSM,+ERFSB} - c_{LSM,ETP}$, and $\Delta c_{HSM} = c_{HSM,+ERFSB} - c_{HSM,ETP}$.

The c_{LSM} shows a slight dependence on temperature, whereas Δc_{LSM} does not depend on the substrate temperature. The c_{HSM} and Δc_{HSM} show a clear dependence on the substrate temperature. Employing an ERFSB results in a reduction of the c_{HSM} for $T_{sub}<250$ °C at condition A and a reduction of c_{HSM} for $T_{sub}<350$ °C at condition B.

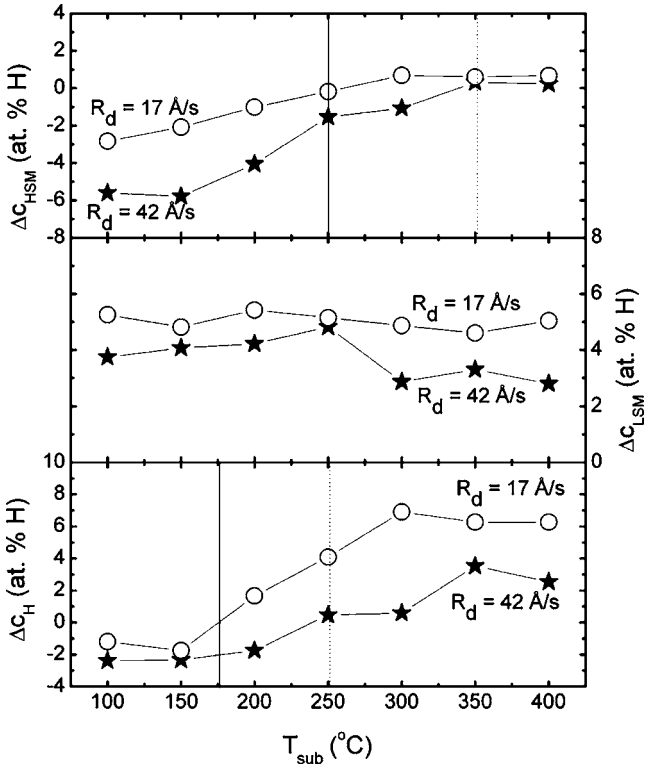

FIG. 11. The change in hydrogen content contributing to the HSM and LSM, Δc_{HSM} and Δc_{LSM}, respectively, and the change in the total hydrogen content Δc_H due to ERFSB (V_{dc}=−60 V) vs the substrate temperature for condition A (open circles) and condition B (solid stars).

For $T_{sub}<175$ °C (condition A) and $T_{sub}<250$ °C (condition B) the total hydrogen content is smaller with ERFSB (see Figs. 10 and 11). The opposite is observed for $T_{sub}>175$ °C (condition A) and $T_{sub}>250$ °C (condition B), for which the total hydrogen content is higher under ERFSB.

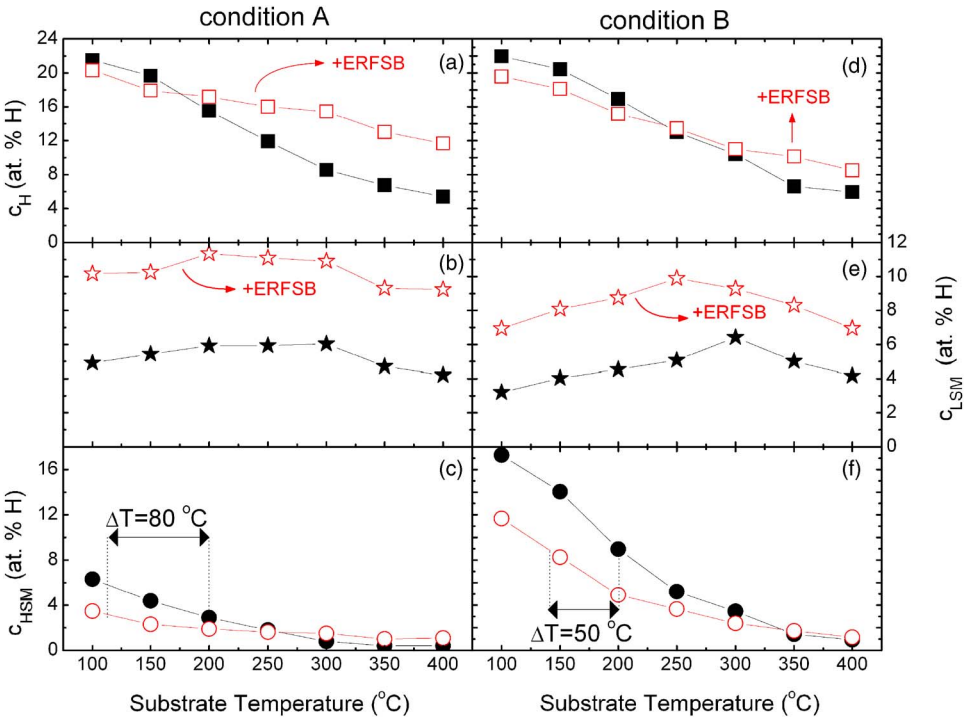

FIG. 10. (Color online) The total hydrogen content c_H (squares), the hydrogen content contributing to the LSM c_{LSM} (stars), and the hydrogen content contributing to the HSM c_{HSM} (circles) vs the substrate temperature for R_d=11 Å/s (condition A) [(a)–(c)] and R_d=25 Å/s (condition B) [(d)–(f)] without ERFSB (solid marks) and with ERFSB (open marks).

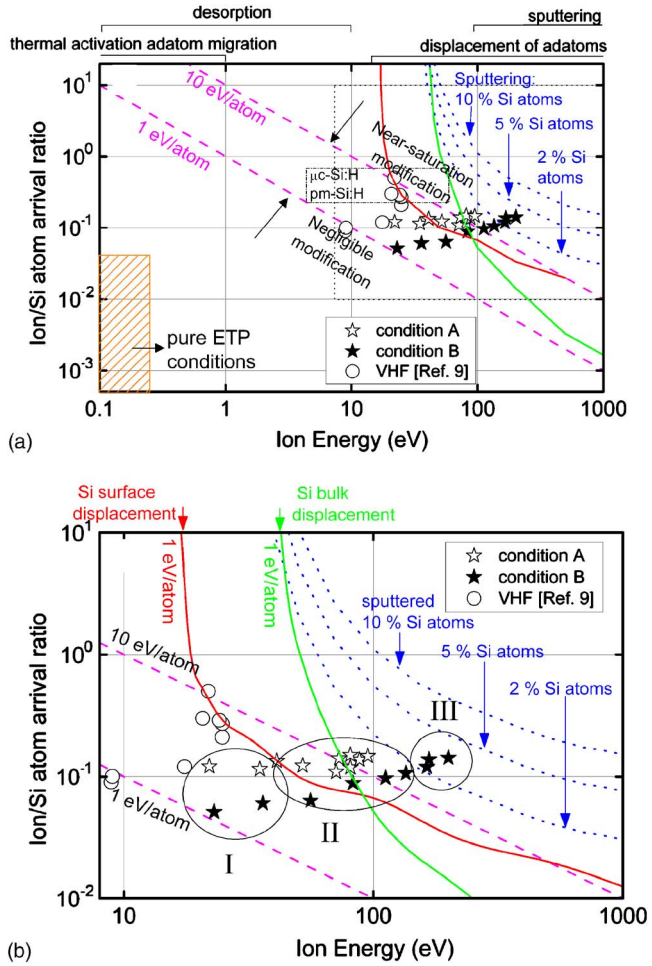

FIG. 12. (Color online) (a) The ion-film interaction diagram of ion/atom arrival rate vs the ion energy (adapted from Ref. 17). The dashed lines confine the area in which property modification of thin film deposition is expected. The shaded area reflects the area for *a*-Si:H growth under ETP without ERFSB conditions. The ETP depositions with ERFSB as reported in this paper are presented by the open stars (condition A) and the solid stars (conditions B). The open circles correspond to the VHF-CVD conditions adapted from Ref. 9. The kinetic ranges of atoms and ions where significant ion-surface (displacement and sputtering) or vapor-surface (thermally activated surface migration and desorption) interactions occur (adapted from Ref. 18) are also shown at the top of (a). (b) A close-up of the most relevant part of the ion-film interaction diagram of *a*-Si:H growth. The dotted lines correspond to the specific ion/atom arrival rate and ion energy at which 2%, 5%, and 10% of the deposited Si atoms are sputtered by Ar^+ ions as calculated using the analytical function in Ref. 20. The solid lines correspond to the ion/atom arrival ratio at specific ion energies at which ions deliver on average 1 eV per Si atom by means of Si surface atom and Si bulk atom displacement by means of the solid lines as calculated from the data in Ref. 19. The circles indicate the phases I, II, and III as described in the text.

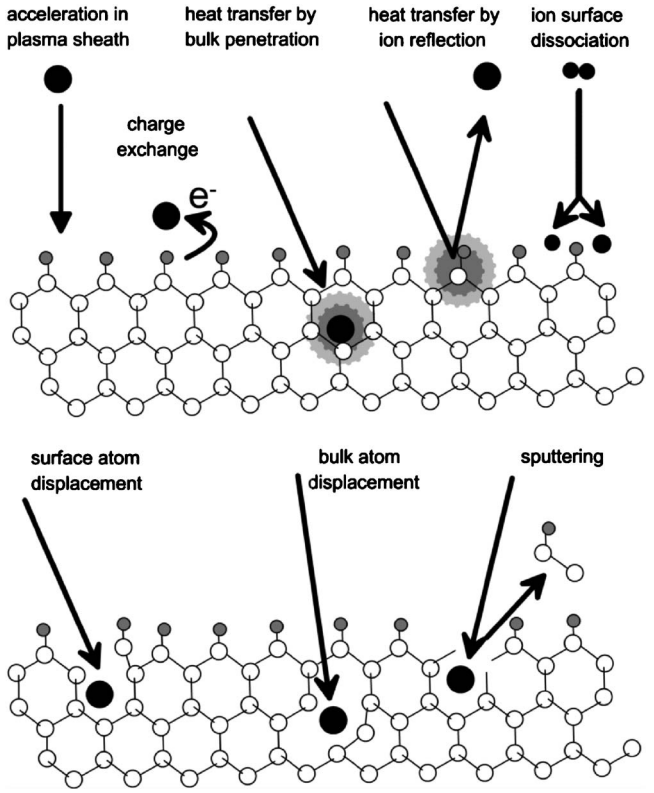

FIG. 13. A visual interpretation of low energetic ion-surface and ion-bulk interactions with a crystalline lattice during thin film growth.

IV. DISCUSSION

A. The ion-film interaction diagram

In this section we introduce an ion-film interaction diagram to streamline the discussion on which ion-induced processes are important for the film modifications presented in Sec. III. In Fig. 12(a) the ion/atom arrival ratio is plotted versus the averaged ion energy. The range in which 1–10 eV per deposited atom is available is depicted in the ion-film interaction diagram between the two dashed lines. In this specific region significant material property changes can be expected for any film growth.[17] As mentioned earlier, Hamers *et al.*[9] showed that with increasing ion energy per deposited Si atom, the film density is increased as well. The corresponding data are included in Fig. 12(a) (open circles) and fit nicely in the range in which 1–10 eV per Si atom is available. The ETP deposition conditions without ERFSB are depicted by the shaded area in Fig. 12(a), and are located in the region of the ion-film interaction diagram in which not the ion-surface interactions but the radical-surface interactions dominate the *a*-Si:H growth. The ETP conditions A and B with ERFSB are depicted in the ion-film interaction diagram with open and solid stars, respectively. The ERFSB results in an additional energy of 5–20 eV available per Si atom deposited compared to *a*-Si:H deposition without ERFSB. Figure 12(a) implies that the ETP with ERFSB conditions is also in the range in which significant property modifications of the film growth can be expected. Typical ion/atom arrival ratios of 10% for the ion energy range of 25–58 eV have been reported for rf-PECVD (Ref. 37) (not shown in Fig. 12). These values are comparable with our ERFSB conditions, whereas compared to the VHF data, the general difference between rf and VHF is reflected by the larger ion energy and smaller ion flux for the rf-PECVD conditions.

First we will consider the low energetic ion-surface interactions which can occur in the regions of *a*-Si:H growth in the ion-film interaction diagram of *a*-Si:H as illustrated in Fig. 13. The ions accelerate and gain energy in the plasma sheath. If the ion arrives at the surface it will be neutralized by means of charge exchange.[38] This process occurs a few angstroms from the surface through an Auger or resonant

tunneling process.[39–41] Even though the high energetic particles arriving at the surface are neutralized, we will keep referring to them as "ions" in this paper. If the ions do not have enough energy to penetrate the bulk they are either adsorbed or scattered back. Both low energetic ion-surface interactions can already result in an energy transfer to the surface in the form of a local thermal spike (note that during the charge exchange also the ionization energy is released). Furthermore, it is speculated that ions below a certain threshold E_p can penetrate below the surface as an interstitial without creating any damage.[38,42] For ions bombarding silicon it is estimated that $E_p \sim 7$ eV.[42] If the ion has enough energy it can displace atoms in the lattice, in which Si surface and bulk displacement (some monolayers underneath the surface) can be distinguished. The threshold energy for surface Si displacement is roughly 18 eV, whereas the threshold energy for the more bonded bulk Si is higher, i.e., roughly 40 eV.[19] At even higher ion energies the atoms can be sputtered away. The threshold energy for Si sputtering is roughly 50 eV and the sputter yield increases drastically with increasing ion energy.[20] Note that all these processes will also result in local thermal spikes to dissipate excess energy on the growth surface or in the bulk.

The close-up of the diagram range of interest to our *a*-Si:H deposition conditions with ERFSB is depicted in Fig. 12(b). In this figure the regions in which sputtering, Si surface atom displacement, and Si bulk atom displacement become important are also shown. The specific ion/atom arrival rate and ion energy at which 2%, 5%, and 10% of the deposited Si atoms are sputtered by Ar^+ ions is depicted by the dotted lines in Fig. 12(b) as well. These lines are calculated from the analytical Si sputter yield dependence on the Ar^+ ion energy as reported in Ref. 20. In Fig. 12(b) we plotted the ion/atom arrival ratio at specific ion energies at which ions deliver on average 1 eV per Si atom by means of Si surface and Si bulk displacement (solid lines). These solid lines are calculated using the data on network damage by surface Si displacement and bulk Si displacement by means of Ar^+ ions. Note that the data for sputtering and displacement are based on Ar^+ ions. As discussed earlier, the most likely ions, which will dominate the surface bombardment under the ETP conditions with ERFSB, are SiH_n^+ ions. The sputter and displacement yield for both ions will be roughly the same since the ion mass does not differ too much (28–31 amu compared to 40 amu),[19] which validates the use of the data based on the Ar^+ ion.

Note that the ion-film interaction diagram reflects the yield of the ion-film interactions under deposition conditions; however, it does not provide information of the penetration depth of the ion-bulk interactions in to the bulk of the film. Nevertheless, in general we can state that the higher the ion energy, the deeper the ion penetration in to the bulk film will be.

The positions of conditions A and B in the ion-film interaction diagram are roughly presented by the open and solid stars, respectively. Note that the data points for conditions A and B in Fig. 12(b) represent the averaged ion energy and that the IED is much broader than reflected by the width of data point in the figure. Furthermore, in the calculation of ion/Si deposition atom arrival ratio it is assumed that the largest fraction of the rf power is mainly consumed in the sheath as kinetic energy. The data reflect a 100% efficient rf-power incoupling. Considering the uncertainties around the efficiency of the rf-power incoupling, the real ion/Si atom arrival ratio could be up to a factor 2 smaller. In spite of these uncertainties, Fig. 12(b) shows that under experimental conditions A and B more ion-induced film interactions are activated with increasing the averaged ion energy. If we look in more detail to the position of conditions A and B in the diagram, we can distinguish roughly three phases: I, II, and III. Phase I corresponds to ion-bombardment conditions in which the dominant ions can only induce a Si surface displacement. Phase II corresponds to ion-bombardment conditions at which the Si bulk displacement also starts to play a role. Phase III corresponds to conditions in which also Si sputtering starts to play a role. The introduced three phases are convenient in discussing the observed ion-bombardment induced film modifications.

B. Relation between the material properties and the ion-film interaction diagram

As mentioned earlier, a small fraction of the ion flux could consist of the hydrogen poor ionic clusters $Si_nH_m^+$ created in the ETP. If an ERFSB is employed, the ionic clusters are accelerated in the plasma sheath and can scatter in to fragments, like Si single atoms, during its impact on the growth surface. Compared to a small ion, the same ion energy is distributed over all Si atoms in the clusters. Per silicon atom originating from a cluster, less energy is transferred to the surface or the bulk compared to a Si originating from a small ion. Therefore, it is unlikely that these large ions can penetrate into the bulk.[43] Since the ionic clusters are only a small fraction of the total ion flux, the majority of the ion energy is transferred to the surface by the smaller ions. Consequently, the ion-induced film modifications of the material properties are caused by the smaller ions. Here we will discuss whether the observed experimental trend can be explained in terms of the ion-film interaction diagram introduced.

The question which we address here is whether, based on the results presented in Sec. III, the ion-surface processes responsible for the microstructural changes of the *a*-Si:H material can be identified. First we will consider the enhancement of the vacancy incorporation under ERFSB. A vacancy is defined as a lattice site at which up to three Si atoms are missing.[33] In *a*-Si:H deposited by means of a pure ETP plasma the *a*-Si:H bulk network contains predominantly divacancies for $c_H < 14$ at. %.[33] The vacancy incorporation mechanism under growth conditions without ERFSB is most probably a mechanism in which the relaxation of the *a*-Si:H network at the surface or subsurface during the *a*-Si:H growth is locally inefficient, in such a way that sites incorporate at which a Si atom is "missing." Here we will discuss whether under ion-bombardment vacancies can be incorporated by means of ion-induced Si atom displacement or ion-induced sputtering of a Si atom in the subsurface or surface region during the growth. The open bonds created at such vacancy sites are passivated by the abundance of hy-

drogen present at the growth surface during *a*-Si:H deposition. Figure 12(b) implies that by increasing the $|V_{dc}|$ the efficiency of the ion-induced Si atom displacement increases (phases I and II). Since sputtering is still ineffective in phases I and II, the enhancement in the vacancy incorporation is a result of ion-induced Si atom displacement. However, the question remains whether the Si atom surface or bulk displacement is responsible for the vacancy incorporation. Since the surface vacancy created by an ion-induced Si surface displacement can be filled again during growth, it is more likely that the bulk displacement rules the additional incorporation of vacancies. Another argument supporting this assumption is the fact that the largest increase in the vacancy density is observed in phase II, the phase in which the Si bulk displacement becomes significantly activated. At maximum 6 at. % H (in c_{LSM}) is more incorporated due to ion bombardment, as shown in Fig. 5. If we assume that under ERFSB divacancies are still the dominant vacancies present in the bulk, this corresponds to ~2 at. % Si atoms, which are displaced in the bulk.

Secondly we will consider the reduction in nanosized void incorporation under ERFSB conditions. The nanosized void incorporation mechanism is based on the fact that surface valleys evolve into nanosized voids during growth. A valley is incorporated as a nanosized void by overhangs that are formed during growth.[25,44,45] As mentioned earlier, nanosized void incorporation is controlled by a competition between the growth flux and the surface diffusion for non-ion-assisted growth conditions.[25] Two possible mechanisms, which can reduce the nanosized void incorporation, are the enhancement of the surface diffusion or sputtering of the overhangs. Both mechanisms are plausible since they also have been observed in molecular dynamics calculations[44,45] of the deposition of an arbitrary film from high energetic particles (corresponding to ions) and low energetic particles (corresponding to neutral or radicals). Enhancement of the diffusion of surface species results in a more efficient filling of the surface valleys and as a consequent less voids are incorporated. The thermal activation energy to bring surface species in a diffusional state is in the order of 0.7–1.1 eV for ETP growth without ERFSB.[25,46] This means that only a small fraction of the ion energy (20–100 eV) has to be transferred to the surface species during the ion-surface interaction. Therefore it is plausible that one single ion-surface interaction can locally excite more than one surface species into a diffusional state. The other mechanism is based upon preventing the overhangs to grow over the valleys. This ion-surface interaction requires a sputtering process. Under the ion impact the initial overhang is sputtered away and the valley can be filled by the precursors arriving and migrating over the surface. As shown in Fig. 5, in phase I the void density ($\sim c_{HSM}$) drops already drastically with $|V_{dc}|$, in phase II the void density decreases slightly with increasing $|V_{dc}|$, and in phase III it increases with $|V_{dc}|$. In line with earlier discussion on the relation between vacancy incorporation and sputtering, the sputtering effect is not very likely to be responsible for the reduction of the void incorporation, since sputtering is not sufficiently activated in phases I and II. As a consequence the enhancement of the surface diffusion is the most plausible mechanism responsible for the reduction in the void incorporation. This conclusion is further corroborated if one considers the fact that the enhancement of surface migration is a process, which in principle smoothens the amorphous surface. We have confirmed *a*-Si:H growth with smoother surfaces under deposition conditions with ERFSB compared to without ERFSB by means of *in situ* spectroscopic ellipsometry studies (not shown in this paper). The fact that the void density drops already drastically in phase I suggests that the ion-induced surface Si displacement, the only activated ion-surface interaction, is most likely to be responsible for this effect.

In phase III the density of nanosized voids increases slightly with $|V_{dc}|$ (see Fig. 5) and Si growth flux shows a 10% reduction (see Fig. 4). This is a result of the sputter effect, which according to Fig. 12(b) starts to play a role in phase III.

The fixed microstructure dependence for depositions without ERFSB as shown in Fig. 6 is mainly a result of the nanosized void incorporation mechanism which as mentioned above is a competition between the surface diffusion (approximate substrate temperature) and the growth flux.[25] Under ERFSB conditions, the ion-surface interactions contribute also to the *a*-Si:H growth and the microstructure breaks out the surface-diffusion-controlled dependence. In other words ERFSB provides us an extra degree of freedom in the variety of *a*-Si:H microstructures which can be obtained.

In phase I also the defect density decreases drastically and the optoelectronic properties improve. The reduction can be explained (1) in terms of the ion-surface and ion-bulk interactions presented in the ion-film interaction diagram; however, (2) a possible effect of the modification of the bombarding ionic clusters under ERFSB on the defect incorporation cannot be excluded.

(1) Since in phase I only surface Si displacement is sufficiently activated, we suggest that this process is beneficial to reduction of defect incorporation. An explanation for the lower defect density could be that ion-bombardment induced Si surface atom displacement prevents the incorporation of features such as strained or weak bonds, which can finally end up as defects in the *a*-Si:H network. The fact that only a moderate ERFSB bias is required to reduce the defects and to improve the conductivity could reflect a relation between the specific defect type removed under ion bombardment and the material's improved opto-electronic properties.

(2) As discussed earlier, ionic clusters are a minority contributor to the ion flux under ERFSB conditions. As shown by Shimizu *et al.*,[4] better stability and lower defect densities are obtained when the fraction of polysilane radicals in the growth flux is reduced. If these ionic clusters are incorporated in the bulk, these clusters could be the origin of the higher defect densities[43] under pure ETP deposition conditions. If an ERFSB is employed, the ionic clusters are accelerated in the plasma sheath, after which they can be dissociated in fragments

containing one single Si atom on the growth surface, preventing the incorporation of a cluster related defect.

If we consider the fact that minimum bulk defect densities have been observed in the same ion energy range for different deposition techniques such as rf- and VHF-PECVD,[13,14] it is most likely that the defect incorporation is ruled by a general process, such as the ion-induced surface Si displacement.

No direct relation between the defect density and the vacancies has been found. Nevertheless, in phase I the nanosized voids (see Fig. 5) seem to behave similarly as the defect density. By employing a moderate ERFSB both parameters decrease drastically in phase I. This resemblance does not imply that both the reduction of voids and the reduction of defects are directly related, or in other words this specific defect does not have to be present at nanosized voids. However, the trend of nanosized voids and defects in phase I could be a result of the same ion-surface interaction, which would be the Si surface atom displacement.

We would like to mention that *a*-Si:H films deposited at high deposition rates by ETP without and with ERFSB have been incorporated in a *p-i-n* solar cell device, as described elsewhere.[47] The optimized efficiency under pure ETP conditions had an initial efficiency of 5.9% at a deposition rate of 11 Å/s. The performance of the solar cell improved up to an initial efficiency of 7.0% with *a*-Si:H films deposited with ERFSB under phase I conditions, i.e., using a moderate ERFSB. The better *p-i-n* performance was mainly a result of the higher short-circuit currents as a result of reduced free carrier recombination at defects in the *i*-layer.

Another aspect to be discussed is to what extent the energy transfer via the ion-surface interactions is interchangeable with substrate temperature. Si bulk displacement is not expected to depend strongly on the substrate temperature. This is in line with the fact that Δc_{LSM}, i.e., the ion related vacancy incorporation, for conditions A and B do not show any significant temperature dependence (see Figs. 10 and 11). The vacancy density increases ($\sim\Delta c_{\mathrm{LSM}}$) more under ERFSB with $V_{\mathrm{dc}}=-60$ V for films deposited at a rate of 17 Å/s (A) compared to the films deposited at 42 Å/s (B). This is in agreement with the ion/atom arrival ratio as depicted in Fig. 12(b). The ion/atom arrival ratio is higher for condition A than for condition B. Under condition A more ions are available per deposited Si atom, which results in more Si bulk displacement. Consequently the c_{LSM} is mainly determined by the V_{dc} and the ion/atom arrival ratio and not by the substrate temperature.

The enhancement of surface diffusion via Si surface displacement can in principle be interpreted as a reduction of the activation barrier to bring surface species into a diffusional state. In other words, the incorporation of nanosized voids is controlled by the substrate temperature, the growth flux, V_{dc}, and the ion/atom arrival ratio. In this process the ion bombardment and substrate temperature are roughly exchangeable. Here we try to express the interchangeability of the substrate temperature and ion energy for ion-surface process responsible for the reduction of the void incorporation. At a typical deposition temperature of 200 °C the ion bombardment at $V_{\mathrm{dc}}=-60$ V corresponds to a reduction in substrate temperature of 50 up to 80 °C, as shown in Fig. 10.

Noteworthy is the fact that the Si surface displacement and the Si bulk displacement have an opposite effect on the total hydrogen content during *a*-Si:H growth, the Si surface atom displacement results in a decrease in the total hydrogen content, and the Si bulk atom displacement results in an increase in the total hydrogen content. The fact that ion-induced Si bulk displacement is independent of substrate temperature is the origin of the extra degree in freedom in the variety of microstructures obtained when an ERFSB is employed (see Fig. 6).

These results imply that as long as the growth occurs under conditions outside phases II and III, ion bombardment and substrate temperature can be exchanged. This means that for low deposition rates $\leqslant 1$ Å/s the available thermal energy at typical deposition temperatures (180–250 °C) is sufficient to deposit "high quality" *a*-Si:H material, without the need of the ion-film interactions. This is corroborated by the highly stable *a*-Si:H films deposited at 0.12–0.18 Å/s using the triode rf-PECVD configuration[4] in which ion bombardment does not play a significant role.

Finally, we would like to address that the ion-film interaction diagram is also applicable for μc-Si:H deposition conditions. For μc-Si:H deposition by rf-PECVD higher pressures are required in comparison to *a*-Si:H growth using rf-PECVD. The effect of deposition at higher pressures is that the ion-bombardment energy is quenched (<15 eV) by ion-neutral collisions in the plasma sheath. Kondo *et al.*[5] showed that the ion energy has to be below *a* certain threshold value to deposit μc-Si:H. Hamers *et al.*[48] showed for rf-PECVD deposition the ion/atom arrival ratio for μc-Si:H deposition conditions was around 0.70, much higher as compared to the ratio $\sim$0.05 found for the *a*-Si:H rf-PECVD conditions. The region in the ion-film-interaction-diagram in which μc-Si:H is deposited is depicted as well. In these H_2 diluted SiH_4 plasma conditions the H_n^+ ($n=1-3$ depending on the pressure) ion becomes the dominant ion, which is less effective in the Si displacement due to its smaller mass. As shown in another paper,[6] the most energetic ions, containing at least one silicon atom, are responsible for the local amorphization in the microcrystalline grains of the μc-Si:H films via the ion-induced Si bulk displacement mechanism.

V. CONCLUSIONS

The effects of additional ion bombardment on the *a*-Si:H material properties generated in an ETP plasma with ERFSB have been studied. Based upon the literature we propose an ion-film interaction diagram, which helps us identify the ion-surface or ion-bulk interactions responsible for the film modifications observed. According to this ion-film interaction diagram, the ETP conditions with ERFSB can be roughly divided in three phases. In phase I the only low energetic ion-surface process activated is Si surface atom displacement. In phase II also the ion-induced Si bulk atom displacement is sufficiently activated, whereas in phase III the ion-induced sputtering also starts to play a role. Phase I is characterized by a reduction in the nanosized void density,

reduction in the defect density, and improvement of the photoresponse. Our results suggest that Si surface atom displacement is a crucial process in these mechanisms; Si surface atom displacement enhances the surface migration. Phase II is characterized by an enhancement in vacancy incorporation. In accordance with the introduced ion-film interaction diagram, we claim that the Si bulk displacement process is responsible for the incorporation of additional vacancies. Phase III is characterized by the decrease in growth flux and the increase in void density. The contribution of sputtering in phase III is responsible for this effect.

The Si surface atom displacement is the only ion-induced process in which the substrate temperature and ion energy are interchangeable. Si bulk displacement and sputtering do not show an interchange relation between substrate temperature and ion energy. Consequently, the ion-induced surface and bulk processes provide an extra degree of freedom in the *a*-Si:H microstructure which can be obtained.

Finally, the ion-film interaction diagram introduced in this paper shows that the efficiency of the Si surface atom displacement process determines the conditions at which best opto-electric *a*-Si:H can be deposited. The typical ion energy has to be 25–40 eV, around ion/atom arrival ratio of 0.1–0.3. This results in conditions in which the additional ion energy provided per deposited Si atom is 5 eV up to 10 eV and the Si surface displacement is sufficiently activated.

ACKNOWLEDGMENTS

The authors thank Agnes Petit for the TR/DBP characterization. The technical assistance of Ries van de Sande, Jo Janssen, Bertus Hüsken, and Herman de Jong is gratefully acknowledged. This work was sponsored by FOM, NOVEM, TDO, and the EET II Helianthos project.

[1]H. Fujiwara, M. Kondo, and A. Matsuda, J. Non-Cryst. Solids **338–340**, 97 (2004).
[2]R. J. Koval, J. Koh, Z. Lu, L. Jiao, R. W. Collins, and C. R. Wronski, Appl. Phys. Lett. **75**, 1553 (1999).
[3]P. Roca i Cabarrocas, A. Fontcuberta, S. Lebib, and Y. Poissant, Pure Appl. Chem. **74**, 359 (2002).
[4]S. Shimizu, M. Kondo, and A. Matsuda, J. Appl. Phys. **97**, 033522 (2005).
[5]M. Kondo, M. Fukawa, L. Guo, and A. Matsuda, J. Non-Cryst. Solids **266–269**, 84–89 (2000).
[6]A. H. M. Smets and M. Kondo, J. Non-Cryst. Solids **352**, 937 (2006).
[7]B. Drevillon, J. Perrin, J. M. Siefert, J. Huc, A. Lioret, G. de Rosny, and J. P. M. Schmitt, Appl. Phys. Lett. **42**, 801 (1983).
[8]B. Drevillon and M. Toulemonde, J. Appl. Phys. **58**, 535 (2004).
[9]E. A. G. Hamers, W. G. J. H. M. van Sark, J. Bezemer, H. Meiling, and W. F. van der Weg, J. Non-Cryst. Solids **226**, 205 (1998).
[10]T. V. Herak, T. T. Chau, S. R. Mejia, P. K. Shufflebotham, J. J. Schellenberg, H. C. Card, K. C. Kao, and R. D. McLeod, J. Non-Cryst. Solids **97&98**, 277 (1987).
[11]M. V. R. Murty and H. A. Atwater, Phys. Rev. B **51**, 4889 (1995).
[12]H. Rinnert, M. Vergnat, G. Marchal, and A. Burneau, Nucl. Instrum. Methods Phys. Res. B **147**, 79 (1999).
[13]P. Roca i Cabarrocas, P. Morin, V. Chu, J. P. Conde, J. Z. Liu, H. R. Park, and S. Wagner, J. Appl. Phys. **69**, 2942 (1990).
[14]A. S. Abramov, A. I. Kosarev, P. Roca i Cabarrocas, M. V. Shutov, and A. J. Vinogradov, Thin Solid Films **383**, 178 (2001).
[15]S. Zhang and D. E. Brodie, J. Phys.: Condens. Matter **3**, 6597 (1991).
[16]K. Kato, S. Iizuka, G. Ganguly, T. Ikeda, A. Matsuda, and N. Sato, Jpn. J. Appl. Phys., Part 1 **36**, 4547 (1997).
[17]H. R. Kaufman and J. M. E. Harper, J. Vac. Sci. Technol. A **22**, 221 (2004).
[18]T. Takagi, J. Vac. Sci. Technol. A **2**, 382 (1984).
[19]Z. Q. Ma, Y. F. Zheng, and B. Liu, Phys. Status Solidi A **169**, 239 (1998).
[20]K. Wittmaack, Phys. Rev. B **68**, 235211 (2003).
[21]E. A. Edelberg, A. Perry, N. Benjamin, and E. S. Aydil, Rev. Sci. Instrum. **70**, 2689 (1999).
[22]V. Dalal, P. Weberger, M. Ring, and P. Sharma, Thin Solid Films **430**, 91 (2004).
[23]M. C. M. van de Sanden, R. J. Severens, W. M. M. Kessels, R. F. G. Meulenbroeks, and D. C. Schram, J. Appl. Phys. **84**, 2426 (1998).
[24]W. M. M. Kessels, R. J. Severens, A. H. M. Smets, B. A. Korevaar, G. J. Adriaenssens, D. C. Schram, and M. C. M. van de Sanden, J. Appl. Phys. **89**, 2404 (2001).
[25]A. H. M. Smets, W. M. M. Kessels, and M. C. M. van de Sanden, Appl. Phys. Lett. **86**, 041909 (2005).
[26]A. H. M. Smets, "Growth related material properties of hydrogenated amorphous silicon," Ph.D. thesis, Eindhoven University of Technology, 2002.
[27]A. H. Mahan, Y. Xu, D. C. Williamson, W. Beyer, J. D. Perkins, M. Vanecek, L. M. Gedvillas, and B. P. Nelson, J. Appl. Phys. **90**, 5038 (2001).
[28]D. Morton, K. J. Boyd, and J. W. Rabalais, J. Vac. Sci. Technol. A **16**, 1321 (1998).
[29]W. M. M. Kessels, M. G. H. Boogaarts, J. P. M. Hoefnagels, M. C. M. van de Sanden, and D. C. Schram, J. Vac. Sci. Technol. A **18**, 2153 (2001).
[30]W. M. M. Kessels, "Remote plasma deposition of hydrogenated amorphous silicon," Ph.D. thesis, Eindhoven University of Technology, 2000.
[31]F. J. H. van Assche, W. M. M. Kessels, R. Vangheluwed, W. S. Mischke, M. Evers, and M. C. M. van de Sanden, Thin Solid Films **484**, 46 (2005).
[32]A. H. M. Smets, W. M. M. Kessels, and M. C. M. van de Sanden, *Amorphous and Nanocrystalline Silicon Science and Technology-2004*, MRS Symposia Proceedings No. 808 (Materials Research Society, Pittsburgh, PA, 2004), pp. A-9–21.
[33]A. H. M. Smets, W. M. M. Kessels, and M. C. M. van de Sanden, Appl. Phys. Lett. **82**, 1547 (2003).
[34]J. P. M. Hoefnagels, Y. Barrell, W. M. M. Kessels, and M. C. M. van de Sanden, J. Appl. Phys. **96**, 4096 (2004).
[35]W. M. M. Kessels, C. M. Leeuwis, M. C. M. van de Sanden, and D. C. Schram, J. Appl. Phys. **86**, 4029 (1999).
[36]I. Kato, Y. Nakano, and N. Yamaguchi, Jpn. J. Appl. Phys., Part 1 **39**, 6404 (2000).
[37]C. Böhm, J. Perrin, and P. Roca i Cabarrocas, J. Appl. Phys. **73**, 2578 (1993).
[38]D. Marton, in *Low Energy Ion-Surface Interactions*, edited by J. W. Rabalais (Wiley, New York, 1994).
[39]H. D. Hagstrum, Phys. Rev. **96**, 336 (1954).
[40]K. Satake and D. B. Graves, J. Vac. Sci. Technol. A **21**, 484 (2003).
[41]T. Gans, V. Schulz-von der Gathen, U. Czarnetzki, and H. F. Döbele, Contrib. Plasma Phys. **42**, 596 (2002).
[42]K. J. Boyd, D. Marton, J. W. Rabalais, S. Uhlmann, and Th. Frauenheim, J. Vac. Sci. Technol. A **16**, 463 (1998).
[43]S. Ramalingam, E. S. Aydil, and D. Maroudas, J. Vac. Sci. Technol. B **19**, 634 (2001).
[44]R. W. Smith and D. J. Srolovitz, J. Appl. Phys. **79**, 1448 (1996).
[45]K.-H. Müller, J. Appl. Phys. **58**, 2573 (1985).
[46]A. H. M. Smets, W. M. M. Kessels, and M. C. M. van de Sanden, Appl. Phys. Lett. **82**, 865 (2003).
[47]A. M. H. N. Petit, V. Nadazdy, A. H. M. Smets, M. Zeman, M. C. M. van de Sanden, and R. A. C. M. M. van Swaaij, Proceeding of the 20th European Photovoltaic Solar-Energy Conference in Barcelona, 2005 (WIP-Renewable Energies, Munich, 2005), p. 1616.
[48]E. A. G. Hamers, A. Fontcuberta, C. Niikura, R. Brenot, and P. Roca i Cabarrocas, J. Appl. Phys. **88**, 3674 (2000).